Analysis of the Thermodynamic Potential of Supercritical Carbon Dioxide Cycles: a Systematic Approach

Francesco Crespi
Giacomo Gavagnin
David Sánchez*
Department of Energy Engineering, University of Seville
Camino de los descubrimientos s/n, 41092 Seville, Spain
crespi@us.es, gavagnin@us.es, ds@us.es

Gonzalo S. Martínez
AICIA
Camino de los descubrimientos s/n, 41092
Seville, Spain
gsm@us.es

After the renewed interest in supercritical carbon dioxide cycles, a large number of cycle layouts have been proposed in literature. These works, which are essentially theoretical, consider different operating conditions and modelling assumptions and thus the results are not comparable.
There are also works that aim to provide a fair comparison between different cycles in order to assess which one is most efficient. These analyses are very interesting but, usually, they combine thermodynamic and technical restrictions which make it difficult to draw solid and general conclusions with regards to which the cycle of choice in the future should be .
With this background, the present work provides a systematic thermodynamic analysis of twelve supercritical carbon dioxide cycles under similar working conditions, with and without technical restriction in terms of pressure and/or temperature. This yields very interesting conclusions regarding the most interesting cycles in literature. Also, useful recommendations are extracted from the parametric analysis with respect to the directions that must be followed when searching for more efficient cycles.
The analysis is based on efficiency and specific work diagrams with respect to pressure ratio and turbine inlet temperature in order to enhance its applicability to plant designs driven by fuel economy and/or footprint.

Nomenclature

sCO_2	Supercritical Carbon Dioxide.
TIT	Turbine Inlet Temperature [ºC].
CSP	Concentrated Solar Power.
WHR	Waste Heat Recovery.
HX	Heat Exchanger.
ε	Heat Exchanger effectiveness.
NTU	Number of thermal units.
$\Delta T_{pinchpoint}$	Pinch Point Temperature Difference.
η_{th}	Thermal Efficiency.
$\eta_{th,O}$	Thermal Efficiency as declared in original paper.
$\eta_{th,GMTS}$	Thermal Efficiency calculated with in-house codes.
$\Delta\%$	Percentage Difference
η_{compr}	Compressor Isentropic Efficiency
η_{turb}	Turbine Isentropic Efficiency
η_{rec}	Recuperator Effectiveness
W_s	Specific work [kJ/kg].
α	Split-flow fraction.
IC	Inter-cooling.
RH	Re-heating.
η_C	Thermal Efficiency of Carnot cycle
T_L	Cycle minimum temperature
T_H	Cycle maximum temperature
CF	Carnot Factor

INTRODUCTION

The interest in the sCO_2 power cycle has increased exponentially in the last years, driven by the unique features of this technology like high thermal efficiency at interme-

*Address all correspondence to this author. Email: ds@us.es

diate temperature, small footprint and great adaptability to different energy sources. Initially proposed by Feher [1] and Angelino [2] in the late 1960s, the sCO_2 power cycle is currently considered for applications such as concentrated solar power, nuclear reactors, oxy-combustion cycles, waste heat recovery, combined cycle power plants and many more. For all of them, a very large number of cycle configurations have been proposed in literature, especially in the last decade.

A comprehensive review of these proposals is available in [3] and also in [4] by the authors. Table 1, excerpted from the latter reference, presentes a total of forty two different configurations along with the declared thermal efficiency and year of publication. Complementarily, a comparison of thermal efficiencies shown in chronological order is provided in Fig. 1, whereas the influence of turbine inlet temperature is presented in Fig. 2. It is visible that the results are very heterogeneous, with cycles operating in very different conditions and with different energy sources. Also, it looks as if each new cycle did not rely on the previously existing body of knowledge, as suggested by the random variation in Fig. 1 where a continuously increasing efficiency over time is lacking.

This observation could arguably be explained by the absence of a thorough and rigorous analysis of the underlying thermodynamics principles of sCO_2 cycles. Indeed, even if a large number of works regarding cycle optimisation have been published, virtually none has followed the path already set forth by Angelino and Feher [1, 5]. Therefore, the objective of the present work is to set up and develop a systematic analysis of the different sCO_2 cycles proposed in literature in order to draw universal conclusions regarding the layouts that are most interesting. To this end, common boundary conditions must be fed into a thermodynamic model of performance along with a similar set of assumptions regarding where the technological limits (maximum pressure) lie. To illustrate this, twelve cycles have been selected amongst those with highest thermal efficiency and the dependence of specific work and efficiency on varying pressure ratio and turbine inlet temperature has been explored. The results are presented in the form of standard diagrams as already employed by Angelino in [5], see Fig. 3, and other authors in literature for open and closed cycle gas turbines [6, 7]. The original idea of Angelino is developed a little further though and applied to the analysis of the twelve cycles at four temperature levels (550, 750, 950 and 1150 ºC) and a significantly larger range of pressures (in certain cases up to 600 MPa). The aim of this approach is to actually separate the thermodynamic potential of each cycle from the inherent technological constraints brought about by the very high operating pressures and temperatures. This is thought to provide a clearer insight into which cycles offer a larger margin for efficiency, should a parallel development of materials, manufacturing and auxiliary systems take place.

SUPERCRITICAL CO_2 CYCLES

The twelve cycles selected to perform the analyses are picked considering their thermal efficiencies averaged by the

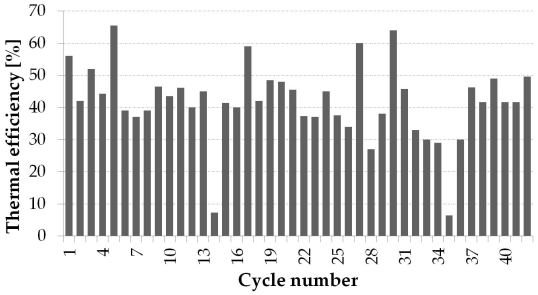

Fig. 1. Chronological evolution of sCO_2 configurations. Cycle numbers refer to Table 1.

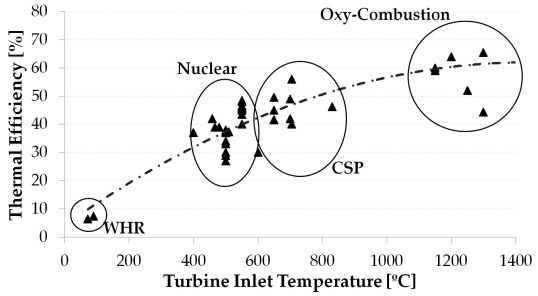

Fig. 2. Dispersion of cycle efficiency against turbine inlet temperature.

characteristic turbine inlet temperatures of their respective applications: nuclear, concentrated solar power and oxy-combustion of natural gas. The reason why thermal efficiency has not been considered as the only figure of merit is that this would have biased the selection towards the cycles used in oxy-combustion applications, with higher turbine inlet temperatures than Nuclear and CSP. At the same time, this criterion avoids considering cycles with very similar layouts. The final selection based on these rationale is presented in Fig. 4. Some comments on this follow.

The *Simple Recuperated* cycle, as originally proposed by Feher [1], is a simple recuperated Brayton cycle adapted to the supercritical region. It is one of the most reviewed layouts in literature with the noteworthy benefit of a much lower compression work thanks to the very low specific volume of the working fluid near the supercritical point. The *Transcritical CO_2* cycle presented by Angelino [2] is a pseudo-Rankine cycle that works with fairly high turbine inlet temperature but very low pressure ratio, thus exhibiting superheated vapour (gas) at the turbine exhaust. Other than this, it presents the same conceptual configuration and benefits as the *Simple Recuperated* cycle. The transcritical *Precompression* layout was also proposed by Angelino [2] and it was later updated by Dostal to a fully supecritical configuration [32]; the same occurred to the *Recompression* and *Partial Cooling* cycles. The interest of the *Precompression* cycle is that the addition of a pre-compressor between the high and low temperature recuperators lifts the restriction posed by the condensation process on turbine expansion ratio.

#	Name	Application	η_{th}[%]	Year	Ref.	#	Name	Application	η_{th}[%]	Year	Ref.
1	Simple Recuperated	Not.spec.	56.0	1968	[1]	22	Hot day	WHR	37.3	2013	[8,9]
2	Transcritical CO2	Nuclear	42.0	1968	[2]	23	Intercooling II	Nuclear	37.0	2014	[10]
3	DEMO	Oxy-comb.	52.0	1995	[11]	24	BraytonCO2GT	CSP	45.0	2014	[12]
4	Matiant	Oxy-comb.	44.3	1999	[13]	25	Reheating II	Nuclear	37.5	2014	[10]
5	Quasi-Combined	Oxy-comb.	65.5	2006	[14]	26	Split-Expansion	Nuclear	34.0	2014	[10]
6	Intercooling I	Nuclear	39.0	2009	[15]	27	Allam + RH	Oxy-comb.	60.0	2014	[16]
7	Reheating I	Nuclear	37.0	2009	[15]	28	Pre-heating	Nuclear	27.0	2014	[10]
8	Double Recompression	Nuclear	39.0	2009	[15]	29	Inter-recuperated	Nuclear	38.0	2014	[10]
9	Recompression	Nuclear	46.5	2011	[2,17]	30	Recuperated CPOC	Oxy-comb.	64.0	2014	[18]
10	Precompression	Nuclear	43.5	2011	[2,17]	31	REC2	Nuclear	45.7	2014	[19]
11	Partial Cooling	Nuclear	46.1	2011	[2,17]	32	Turbine Split Flow I	Nuclear	33.0	2014	[10]
12	Driscoll	Nuclear	40.0	2011	[20]	33	Turbine Split Flow II	Nuclear	30.0	2014	[10]
13	Part. Cool. w/ impr. rec.	Nuclear	45.0	2011	[5,17]	34	Turbine Split Flow III	Nuclear	29.0	2014	[10]
14	Rankine w/ reheat	WHR	7.30	2011	[21]	35	Rankine w/ ejector	WHR	6.40	2014	[22]
15	Cascade	CSP	41.4	2012	[23]	36	CPOC	Oxy-comb.	30.0	2014	[18]
16	TCO	Oxy-comb.	40.0	2012	[24]	37	Forced Cooler	Nuclear/CSP	46.3	2016	[25]
17	Allam	Oxy-comb.	59.0	2013	[26]	38	S-EJ	Nuclear/CSP	41.6	2016	[27]
18	BAS	Nuclear	42.0	2013	[28]	39	RC-EJ	Nuclear/CSP	41.6	2016	[27]
19	Recompression + RH + IC	CSP	48.5	2013	[29]	40	MC-EJ	Nuclear/CSP	41.6	2016	[27]
20	Partial Cooling+ RH	CSP	48.0	2013	[29]	41	Double Reheated Recompr.	Fossil Fuel	49.0	2016	[30]
21	REC3	Nuclear	45.5	2013	[28]	42	Schroder-Turner	Solar	49.6	2016	[31]

Table 1. Survey of sCO_2 cycle layouts published in the public domain. Where two references are provided, the first one indicates the year of first publication whilst the reported thermal efficiency is taken from the most recent source.

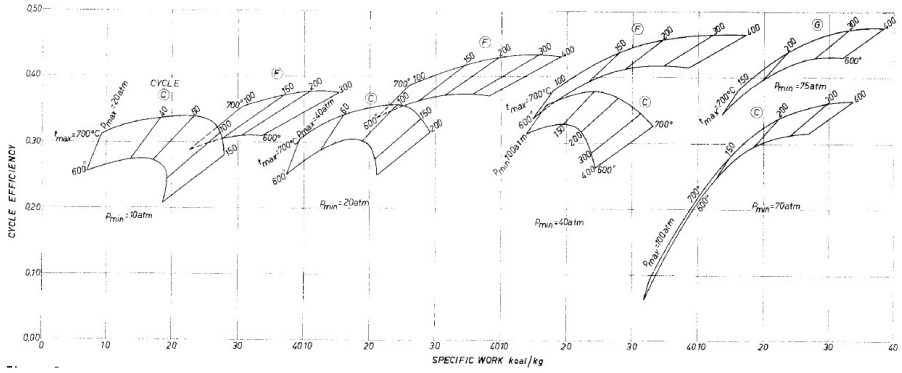

Fig. 3. Thermal efficiency vs Specific Work diagrams originally proposed by Angelino [5].

The *Recompression* cycle [2,32] is named after the (re-) compressor in charge of raising the pressure of the flow that is diverted from the the low-temperature recuperator outlet, in order to balance the heat capacities on both sides of this equipment, Fig. 4. The benefit of this layout is twofold: (i) the pinch-point in the low-temperature recuperator is reduced thanks to the lower mass flow rate on the cold side; (ii) the size of the cooler is reduced thanks to its lower thermal duty. These features lead to a very high thermal efficiency, setting this cycle forth as one of the most interesting sCO_2 layouts in literature.

The *Partial Cooling* cycle is rather similar to the previous one, with the mere addition of a cooler and a pre-compressor before the flow-split valve. The main benefits of this configuration are a higher specific work [17] and a lower sensitivity of global efficiency upon departures from the optimum pressure ratio [33]. The *Recompression + RH + IC* and *Partial Cooling + RH* cycles, realised by simply adding intercooling and reheat to their respective base configurations, have been proposed by Turchi for CSP applications [29]. The *Schroder-Turner* cycle, named after its inventors, is an evolution of the *Partial Cooling* cycle. It results to be an extremely recuperative cycle that exploits the dissimilar specific heats of the various streams created by several flow divisions. In an

alternative embodiment corresponding to the optimum case according to Schroder [31], the one actually considered in the present work, the cycle is slightly simplified by removing the low-temperature recuperator. The *Double Reheated Recompression* cycle presented by Mecheri and Le Moullec [30] is an evolution of the *Recompression* layout with the addition of two reheats. Alternatively, a by-pass valve can be added before the low-temperature recuperator so that a fraction of sCO_2 is bled from the main stream, heated up in another heater and re-injected before the high-temperature recuperator, in order to overcome the usual pinch-point problems.

The *Allam* cycle, named again after its lead inventor, is an oxy-combustion cycle that operates on natural or synthetic gas fuel burnt with pure oxygen produced by an Air Separation Unit. The benefits of this configuration are a very high thermal efficiency and the production of pipeline-ready CO_2 without the need of an auxiliar chemical process [26]. The *Matiant* cycle, invented by Mathieu and Iantovsky [13], is another oxy-fired cycle capable to produce pipeline ready CO_2. As a characteristic feature, the layout presents three expanders, one of them situated halfway through the heating process. Finally, the *Quasi-Combined* configuration is an oxy-combustion cycle proposed by Zhang and Lior [14] and characterised by a rather complex layout with a large number of components, Fig. 4. The stream from the low pressure turbine exhaust to the water separator acts as a sort of energy source (Brayton-like "topping cycle" according to [14]) for the pure sCO_2 flow which can in turn be regarded as the corresponding Rankine-like "bottoming cycle". Due to this particular integration, the cycle is named *Quasi-Combined* by the inventors [14].

SIMULATION TOOLS

In order to analyse the cycles presented in the previous section, in-house Matlab models have been developed on the principal assumption that the working fluid is pure CO_2. This assumption is not formally correct for oxy-fired cycles (cycles j, k and l in Fig. 4), which typically work with a mixture of CO_2, H_2O and residuals in the turbine and low pressure side of the recuperator. Nevertheless, the corresponding inaccuracy (i.e., the impact of the modified composition on turbine work and heat exchanger performance) is considered to not have a large enough influence on the cycle whilst, at the same time, it simplifies the calculations and enables considering these cycles for externally fired applications. For the calculation of the thermodynamic properties of sCO_2, the open-source library *CoolProp* has been used [34].

Heat Exchangers

The heat exchangers have been simulated with a one-dimensional model whereby the equipment is divided in a suitable number of sub-heat exchangers in order to consider small temperature changes and therefore constant sCO_2 properties in each of them [35]. This common expedient enables the application of simplified performance analysis methods like, for instance, the ε-NTU methodology in each division [36]. Other approaches used in literature are even simpler, assuming constant effectiveness or constant ΔT_{min} (pinch-point) at one end of the heat exchanger. In the present work, an initial value of $\varepsilon = 95\%$ is assumed for all divisions and the corresponding temperature differences between hot and cold fluids (ΔT_i) are computed. The resulting minimum difference (pinch point of the heat exchanger ΔT_{min}) is checked to be not lower than 5 ºC. If this were not the case (i.e., $\Delta T_i < 5$ ºC for any given i), the corresponding ε_i would be reduced to achieve the target pinch point.

Turbomachinery

Turbomachinery performance models are fairly simple given that the code is intended for on-design thermodynamic performance only, for which isentropic efficiencies or equivalent figures of merit of the compression/expansion process serve the purpose. Table 2 shows the isentropic compressor/turbine efficiencies reported in (or reverse-calculated from) the original references. Given the large differences observed, it is decided to use a representative polytropic efficiencies for compressors (89%), turbines (90%) and pumps (83%), which then yield different isentropic efficiencies depending on the operating conditions of each turbomachine. The choice of a constant polytropic in lieu of isentropic efficiency is made in order to better capture the influence of the very different pressure/temperature ratios of the cycles considered.

Split-Flow Definition

In literature, the split-flow (or part-flow) fractions (α) are defined in order to attain highest thermal efficiency or, alternatively, to match the temperatures of two streams that mix at a particular location (thus reducing thermal stresses on the component). Nevertheless, these α's apply to a fixed set of boundary conditions and, when the latter change, they must change accordingly. During verification of the code, the values of α are set to those reported in the original papers. Then, for the sake of the simulations in this work, they are modified to yield highest thermal efficiency η_{th}.

Verification

In order to validate the models, a comparison between the performances reported in the original references and those computed by the code is presented in Table 2 and Fig. 5. It is observed that the calculated thermal efficiencies (η_{th}) are very similar to the original values ($\eta_{th,0}$) for cycles from *a* to *i*, with deviations ($\Delta\%$) smaller than 1%. For the oxy-fired cycles, the deviation is slightly larger, the reason being the cited assumption about the composition of the working fluid. Actually, as checked by the authors, these deviations become negligible when specific simulations are run with corrected fluid compositions across the cycle as per the corresponding oxycombustion stoichiometry. This is confirmed by cases *j* and *j2* in Table 2 which correspond to the same *Allam* cycle with pure CO_2 and oxycombustion products respectively; whereas the error in the later is negligible, the calculated ef-

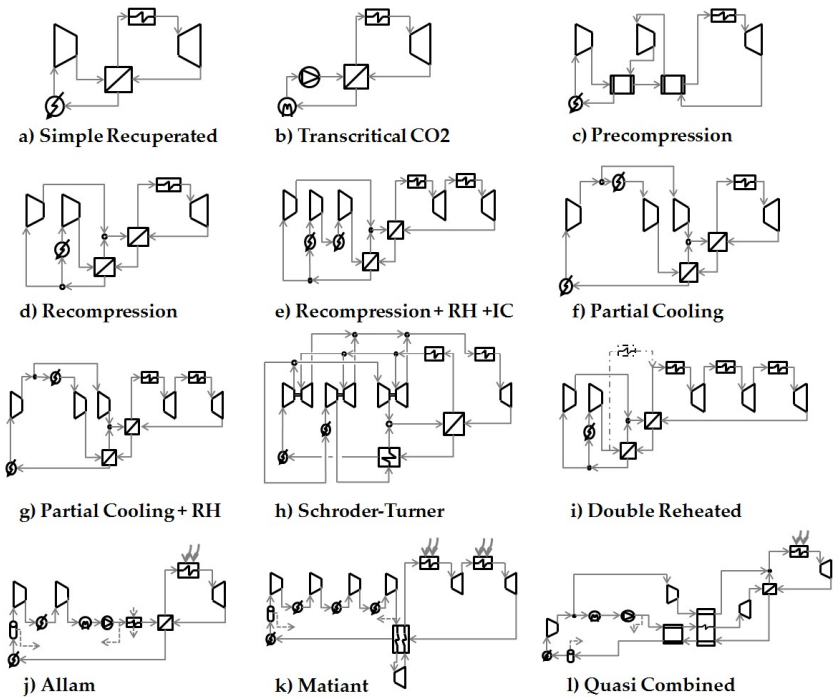

Fig. 4. Summary of cycle layouts.

ficiency in the former is 8% lower than in the reference case. The verification confirms that the code is accurate and can be used in this fundamental analysis.

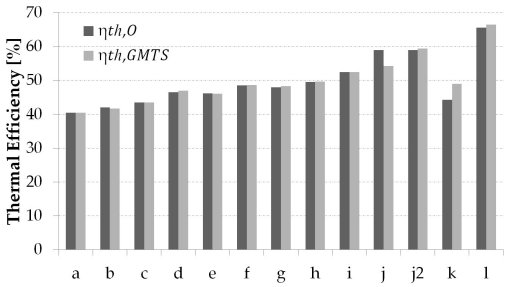

Fig. 5. Verification of the code: comparison between original ($\eta_{th,0}$) and computed thermal efficiencies (η_{th}).

Cycle	η_{compr}	η_{turb}	η_{rec}	$\eta_{th,0}$	η_{th}	Δ%
a	89	93	95	40.44	40.45	0.02
b	85	90	95[1]	42.00	41.63	0.88
c	89	93	95	43.49	43.45	0.09
d	89	90	95/93	46.48	46.98	1.07
e	89	93	95	46.12	46.11	0.02
f	89	93	95	48.50	48.62	0.25
g	89	93	95	48.00	48.31	0.65
h	85/88	93/89	96/98	49.57	49.65	0.16
i	89	93	$\Delta T_{pinchpoint}$ = 6 ºC	52.40	52.42	0.04
j	85	88	95[1]	59.00	54.22	8.10
j2	85	88	95[1]	59.00	59.40	0.68
k	75/85	87	95[1]	44.30	48.99	10.5
l	88	88	90[2]	65.60	66.42	1.25

Table 2. Verification of the simulation code employing the efficiencies reported in literature (η_{compr}, η_{turb} and η_{rec}). Note that, for the *Simple Recuperated* cycle *a*, reference [17] is used instead of [1] and that all the values in the table are displayed as percentages.

Boundary Conditions and Complementary Assumptions

In order to achieve comparable results, the selected cycles have been analysed under the common set of boundary conditions reported in Table 3. Regarding compressor inlet conditions, the standard literature values (32 ºC and 7.5 MPa) are used for the *Simple Recuperated*, *Precompression* and *Recompression* cycles (including the alternative embodiments *e* and *i*). The *Partial Cooling* and related cycles (*g* and *h*) show a lower minimum pressure due to the presence of a pre-compressor, whilst the *Transcritical* CO_2 (*b*) layout presents lower compressor inlet pressure and temperature to

[1] Value not declared in the original papers. The authors have assumed the standard value of 95% from literature.

[2] Heat exchanger effectiveness is not reported in [14] . The authors have found that an effectiveness of 90 % provides the best fit with the values declared in this reference.

enable condensation. Finally, the original paper conditions are used for the oxy-fired cycles (*j*, *k* and *l*).

Pressure drops are set to 1% across each heat exchangers (recuperators, coolers and heaters) whereas piping pressure drops have been neglected and heat exchanger effectiveness takes the default value of 95% (90 % for the *Quasi-Combined* cycle) whenever possible. As said, for those cases where the minimum temperature difference between fluids results lower than 5 ºC, the effectiveness has been reduced in order to match this desired minimum pinch-point.

Cycle	$T_{in,compr}$ [ºC]	$P_{in,compr}$ [Mpa]	$\eta_{pol,T}$ [%]	$\eta_{pol,C}$ [%]	$\eta_{pol,pump}$ [%]	ΔP_{HX} [%]
a	32	7.5	90	89	83	1
b	15	5	90	89	83	1
c	32	7.5	90	89	83	1
d	32	7.5	90	89	83	1
e	32	7.5	90	89	83	1
f	32	5	90	89	83	1
g	32	5	90	89	83	1
h	32	5	90	89	83	1
i	32	7.5	90	89	83	1
j	20	3	90	89	83	1
k	29	0.1	90	89	83	1
l	-70	0.1	90	89	83	1

Table 3. Parameters used in the sensitivity analysis. Note that turbomachinery efficiency is polytropic.

each layout and set of operating conditions. As observed, the plots are made up of two segments with black (full) and white (empty) markers. Black markers correspond to cycles where peak pressure is not higher than 40 MPa whereas white markers indicate that the peak cycle pressure is above this value. This threshold value of maximum cycle pressure is higher than the values usually employed in literature, 25-30 MPa [10, 16], but it is still taken as a representative technological limit for next generation power plants .This is based on the demonstrated operation of supercritical steam power stations at 35 MPa as early as 1960 [37] and on the foreseen increase in live steam pressures in the decades to come [38]. Therefore, the black markers stand for conditions that are currently feasible technology-wise whereas empty markers correspond to scenarios that are valid from a theoretical standpoint only.

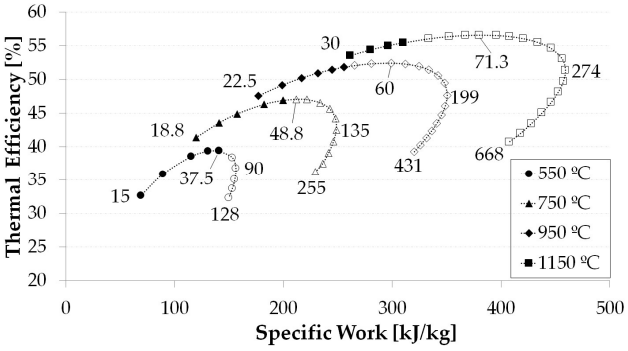

Fig. 6. η_{th} vs W_s diagrams for the *Simple Recuperated* cycle.

RESULTS

Analysis of Individual Cycles

The performances of the aforedescribed cycles have been studied at four different turbine inlet temperature levels -550, 750, 950 and 1150 ºC- and variable pressure ratio. The lower boundary of the temperature range is taken after Angelino's statement that steam Rankine cycles are more efficient than their supercritical CO_2 counterpart for peak temperatures below 550 ºC. The upper boundary is set to a reasonable value that is well above what contemporary heat exchangers can achieve (note that these cycles are mostly intended for externally fired applications). For pressures, the cycle pressure ratio is varied from virtually no compression to the maximum stable pressure (even if this turns out to be ridiculously high). The thermodynamic limits are therefore not fixed arbitrarily by the authors, but they are specific to each cycle configuration and come usually determined by the recuperation process. In other words, the sensitivity analysis to pressure ratio is limited by the pressure ratio for which heat transfer in the recuperators is feasible.

The curves plotted in Figs. 6 to 17 result from the computation of thermal efficiency and specific work for

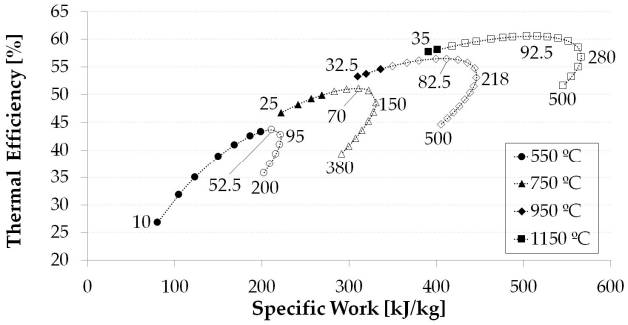

Fig. 7. η_{th} vs W_s diagrams for the *Transcritical CO2* cycle.

Each plot in the diagram shows three or four labels indicating maximum cycle pressure for certain operating conditions. These values are reported for the first and last calculations (i.e., cycles with minimum and maximum peak pressure levels) and for the cases yielding highest thermal efficiency and specific work (even if this last value is not reported in cases where very high pressure ratios are not

feasible). Quoting peak pressure has been preferred over pressure ratio as the latter value is not directly related to the mechanical capability of the system components (note that compressor inlet pressure is different for each cycle and thus there is no univocal correspondence between pressure ratio and peak cycle pressure). It is also worth noting that some curves present a relatively high first value, for instance 34.5 MPa for *Recompression+IC+RH* (Fig. 10) or 40.5 MPa for *Partial Cooling* (Fig. 11). Even if this is partially due to the inherently higher compressor inlet pressures, the main reason is that the curves have been trimmed to avoid intersections between different lines.

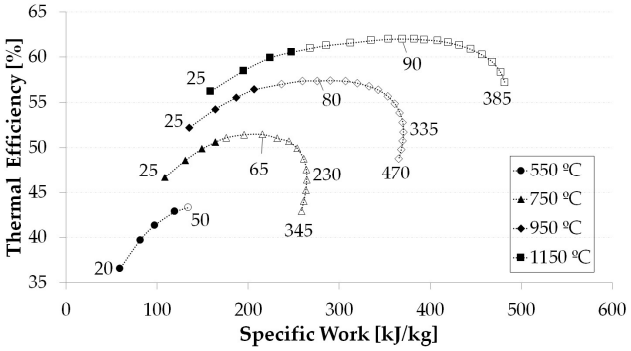

Fig. 8. η_{th} vs. W_s diagrams for the *Precompression* cycle.

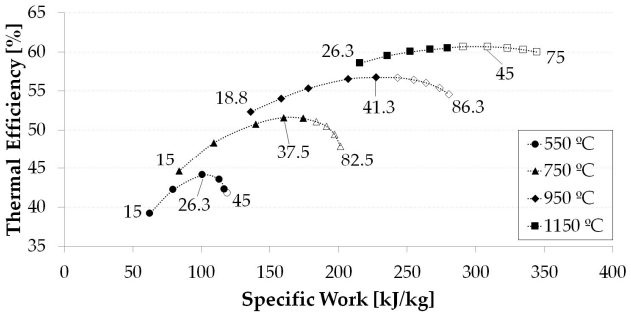

Fig. 9. η_{th} vs. W_s diagrams for the *Recompression* cycle.

Interestingly, the shape of the η_{th} vs. W_s curves changes significantly depending on the configuration considered and the same happens to the maximum cycle pressure. Yet, it is possible to observe several affinities between cycles characterised by similar layouts or thermodynamic features. The *Recompression+IC+RH* and *Double Reheated Recompression* layouts stem from the common root of the *Recompression* cycle, what can easily be observed in the similar patterns presented by Figs. 9, 10 and 14. The same consideration is applicable to the *Partial Cooling* and *Partial Cooling+RH* layouts, which are characterised by the

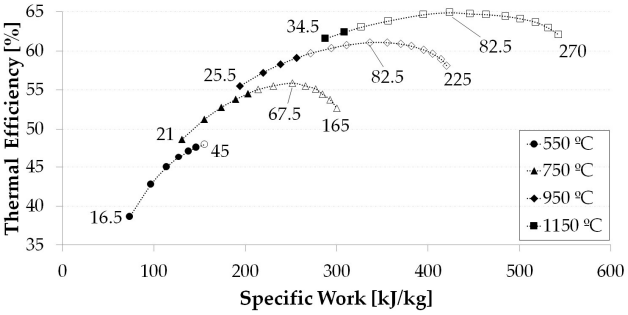

Fig. 10. η_{th} vs. W_s diagrams for the *Recompression+RH+IC*.

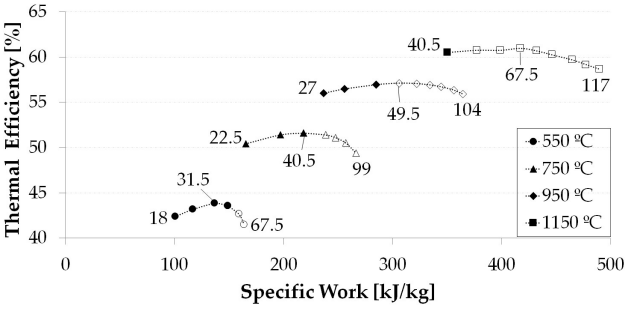

Fig. 11. η_{th} vs. W_s diagrams for the *Partial Cooling* cycle.

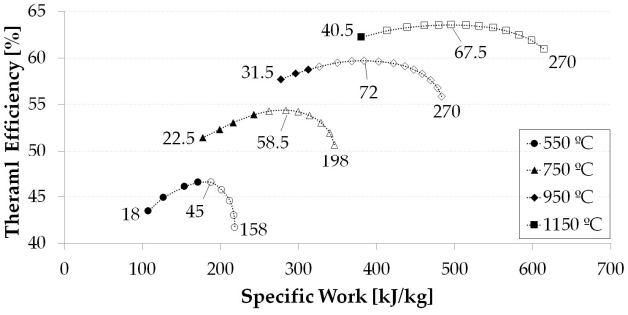

Fig. 12. η_{th} vs. W_s diagrams for the *Partial Cooling + RH* cycle.

same plateau-type trend, especially at high temperatures, or the oxy-fired *Matiant* and *Quasi-Combined* cycles, whose corresponding plots seem to fold back on themselves sharplier. Interestingly, most of these trends are in line with those already discussed by Frutschi in [7] for closed cycle hot-air turbines.

Some common features shared by all the cycles in the comparison are worth noting. For instance, the plots corresponding to lower turbine inlet temperatures seem to have a more circular shape and they turn elliptical and flatter when temperature increases. Regarding the technological limits, it is confirmed that most cycles reach their peak thermal efficiency (and thus specific work) at pressures higher than 40 MPa when turbine inlet temperature is higher than 550ºC. On the contrary, when this temperature is lower than 550ºC,

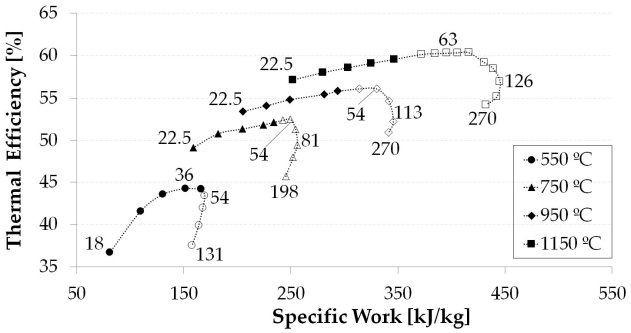

Fig. 13. η_{th} vs. W_s diagrams for the *Schroder-Turner* cycle.

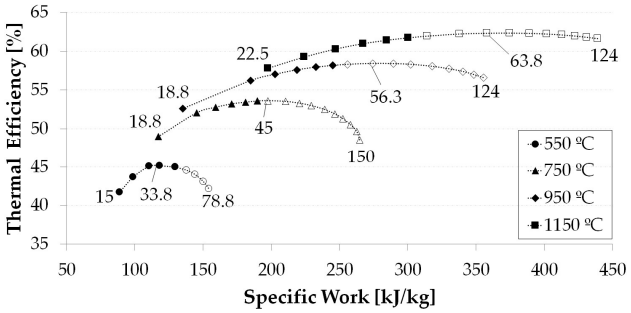

Fig. 14. η_{th} vs. W_s diagrams for the *Double Reheated Recompression* cycle.

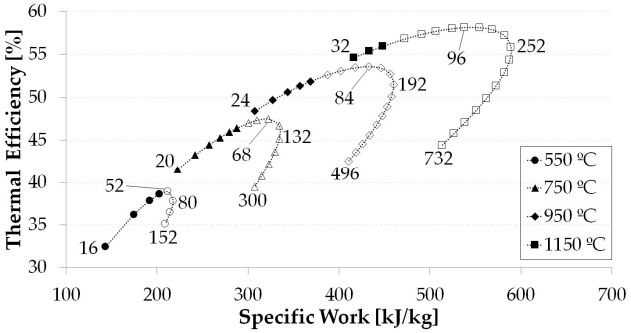

Fig. 15. η_{th} vs. W_s diagrams for the *Allam* cycle.

some cycles achieve peak efficiency within the *feasible* pressure limits (Figs. 6,8,9,11,13,14,17) whilst others do not. Remarkably, the *Quasi-Combined* cycle is the only configuration presenting diagrams almost fully situated within the technological limitations (black markers), mainly due the relatively low pump inlet pressure (Fig. 17).

Compared Analysis

A global assessment of the individual plots shown in the foregoing section suggests that some of the cycles still hold a non-negligible potential for further efficiency increase whereas others seem to have already achieved the best performance possible for a given turbine inlet

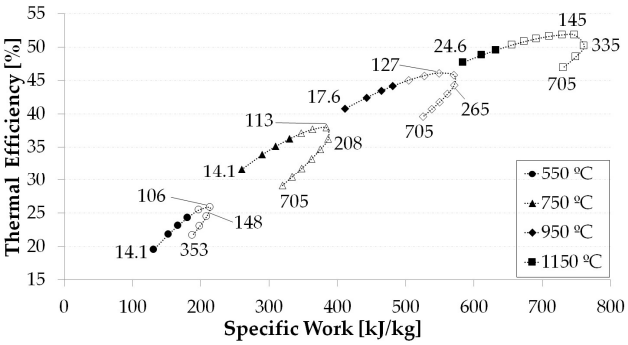

Fig. 16. η_{th} vs. W_s diagrams for the *Matiant* cycle.

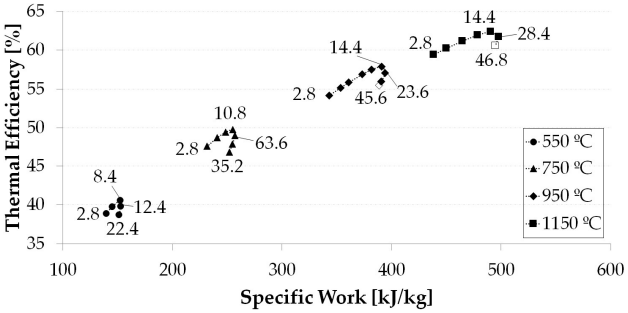

Fig. 17. η_{th} vs. W_s diagrams for the *Quasi-Combined* cycle.

temperature, all this for the current limits of technology. For instance, the *Transcritical* CO_2 cycle operating at 750ºC turbine inlet temperature would be able to attain efficiencies higher than 50% with a very high specific work, yielding fuel and footprint savings simultaneously. Such result sets the thermodynamic road-map for further cycle development, notwithstanding the very high pressures that would be required (∼75 MPa). At the same time, cycles acknowledged to be most efficient, like the *Recompression* layout, seem to have already achieved the highest efficiency for the current turbine inlet temperatures, thus holding no further gains coming from higher operating pressures.

An interesting, not obvious question to answer is which the most efficient or most compact cycle is for a given turbine inlet temperature (energy source). In order to provide a sensible answer to this question, this section presents a comparison amongst the various layouts discussed earlier which are overlaid on one single chart for each temperature level. This is shown in Figs. 18 to 19 where some plots have been trimmed to simplify the reading. The increasing ranges of the horizontal and vertical scales for increasing inlet temperature must be noted.

Let the chart corresponding to 550ºC be considered, Fig. 18. Those cycles conceived for oxy-fired applications (if stable oxy-combustion at such temperature is possible at all) like the *Allam* and, especially, *Matiant* cycles are not of much interest as they exhibit fairly low thermal efficiency in

spite of a very high specific work (small footprint). For this peak temperature, the highest specific work corresponds to the *Allam* cycle if mechanical limits are set on the operating pressure, and the *Transcritical* CO_2 if higher pressures are allowed. With respect to efficiency, the *Partial Cooling + RH* and *Recompression+IC+RH* layouts attain highest efficiencies (46.5 and 47.6% respectively) when pressure is limited to 40 MPa whereas efficiency rises to a higher value (48%) for the *Recompression+IC+RH* cycle if this limit is released. Moreover, from a global standpoint, the *Partial Cooling+RH* and *Transcritical* CO_2 cycles provide a good compromise between thermal efficiency and specific work. In summary, Fig. 18 confirms that the most interesting cycles are *Recompression*, *Double Reheated Recompression*, *Recompression+IC+RH*, *Partial Cooling+RH*, *Transcritical* CO_2 and, in terms of specific work only, the *Allam* cycle.

Increasing turbine inlet temperature brings about changes in the absolute thermal efficiency and specific work achieved by each cycle and also in their relative position in the η_{th} vs. W_s diagram. This is easily observed by comparing the two graphs in Fig. 18. In the plot on the right, corresponding to 750 ºC, the *Matiant* cycle exhibits highest specific work but this feature is offset by a very low thermal efficiency. The *Allam* cycle follows behind with a slightly lower specific work but higher thermal efficiency. Nevertheless, both oxy-fired cycles are still burdened by a low turbine inlet temperature and cannot compete against most of the cycles in the comparison. Considering thermal efficiency only, the scenario remains the same as for 550ºC. The *Recompression+IC+RH* cycle achieves highest η_{th}, 54.5 and 55.8% depending on whether or not pressure limits are in place. The *Double Reheated Recompression* and *Partial Cooling + RH* layouts follow close behind, enabling efficiencies of almost 54%. Overall, the cycles indicated in the previous paragraph remain the most interesting options.

550 ºC would be typical of a Waste Heat Recovery (WHR) application, or even a state-of-the-art Concentrating Solar Power (CSP) plant using molten salts, whereas 750 ºC would represent nuclear applications in Gen IV High Temperature Gas Reactors (HTGR). 950 ºC is a very interesting temperature level as this is currently foreseen for next generation CSP applications using central receiver technology. The resulting performances at this temperature are shown in Fig. 19 where the corresponding plots for each cycle are observed to concentrate on a smaller region of the η_{th} vs. W_s diagram. Regarding oxy-fired cycles, the *Matiant* cycle shifts rightwards to attain very high specific work even if still with the lowest efficiency amongst the cycles considered. When pressure is limited to 40 MPa, the *Partial cooling+RH* layout stems as the most efficient although with moderate specific work, being later matched in efficiency by the *Recompression+IC+RH* cycle when no pressure limit exists; it is noteworthy that the latter cycles can achieve almost 60% efficiency at 950ºC only. Globally, the cycles of interest at this temperature are the *Recompression*, *Double Reheated Recompression*, *Recompression+IC+RH*, *Partial Cooling+RH*, *Transcritical* CO_2, *Quasi-Combined* and, again only in terms of specific work, the *Allam* cycle.

The last chart is Fig. 19 which corresponds to 1150 ºC turbine inlet temperature. It shows similar patterns to Fig. 19 but with higher efficiency and specific work, in particular the latter. The are two main takeaways in this chart. The first is that whilst the achievable efficiency for the given pressure limit of 40 MPa is just over 62%, some of the cycles have the potential to raise this value to almost 65%, which is remarkable for a fairly moderate inlet temperature. The second is related to the *Quasi-Combined* cycle which shifts "north-east" from its initial position in Fig. 18 to a relative position in Fig. 19 where it begins to outperform all the other configurations. This circumstance modifies the overall scenario, as a result of which the most interesting cycles turn out to be the *Precompression*, *Recompression+IC+RH*, *Partial Cooling+RH*, *Transcritical* CO_2, *Allam* and *Quasi-Combined* layouts. Actually, the latter yields the best combination of thermal efficiency (63%) and specific work ($\sim$475 kJ/kg) amongst the portfolio of cycles in this work. This is a very interesting finding as one could have overlooked the true potential of this layout if having the information in Fig. 18 only, which comes to highlight the interest of the parametric analysis shown in the paper.

Further Mechanical Limitation

An interesting analysis from a practical standpoint is to consider another mechanical constraint with regards to the hot inlet temperature of the higher temperature recuperator. To assess this effect, the operating temperature of this equipment is limited to 800 ºC which is higher than for state-of-the-art equipment made of stainles steel (675 ºC) but still compatible with more advanced materials such as Inconel 625 [39].

When this restriction is applied to a turbine inlet temperature of 950ºC, Fig. 19(a) transforms into Fig. 20 where some of the formerly feasible pressure ratios are not feasible anymore. For instance, the *Recompression+IC+RH* and *Double Reheated Recompression* cycles cannot satisfy the new requirement for any pressure ratio, due to the reduced expansion ratio of the last turbine caused by the reheating process; therefore, the corresponding curves are removed from the chart. Also, the *Partial Cooling+RH* layout complies with the new constraint for pressures higher than 40.5 MPa only, which means that they are at the very end of what is considered technically feasible today (and most likely economically unfeasible). Considering 1150 ºC, Fig. 21 represents the new scenario and the dramatic difference is immediately observed by comparing the latter chart with Fig. 19(b). At this high turbine inlet temperature, only three cycles comply with the new mechanical constraint: *Quasi-Combined*, *Transcritical* CO_2 and *Allam*.

These observations confirm the conclusion obtained in the previous section, i.e. that the *Quasi-Combined* and *Partial Cooling+RH* cycles are the most interesting cycles at intermediate to high temperature levels. The interest and ver-

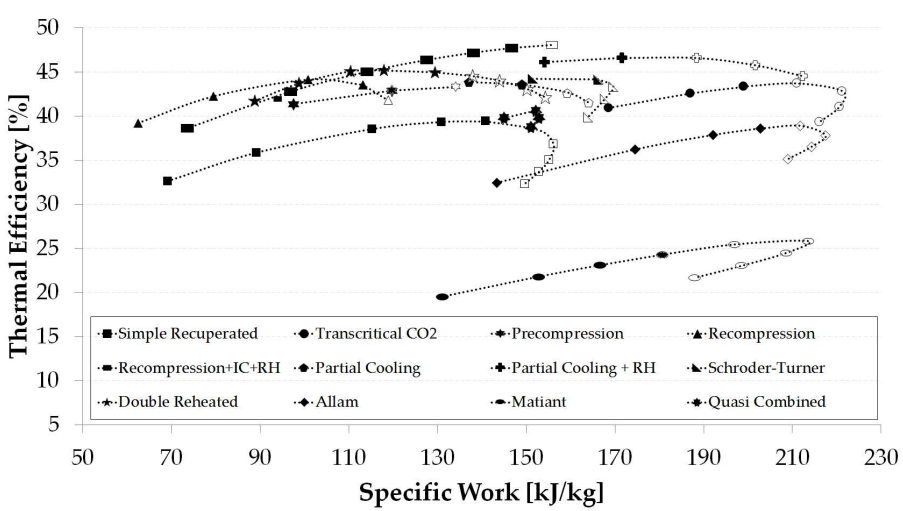

(a) Comparison of cycles operating at TIT=550 ºC.

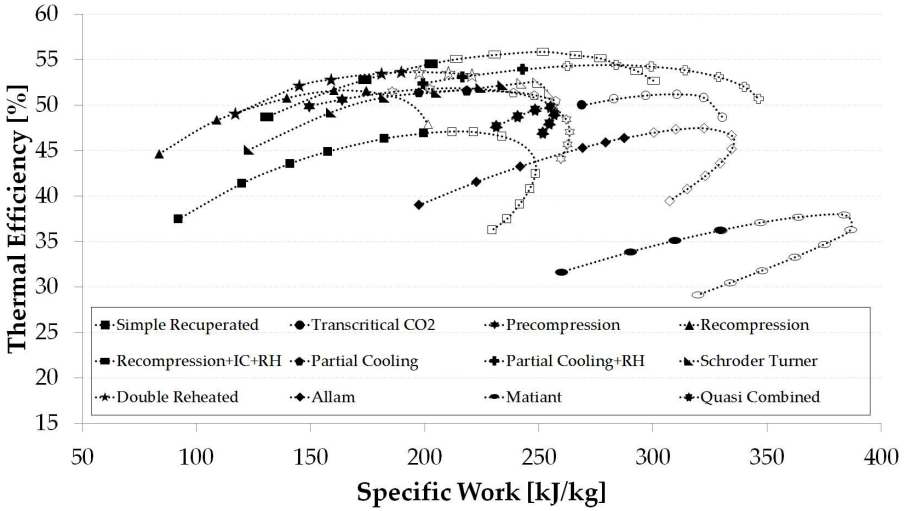

(b) Comparison of cycles operating at TIT=750 ºC.

Fig. 18. Comparison of cycles operating at TIT=550 ºC and TIT=750 ºC.

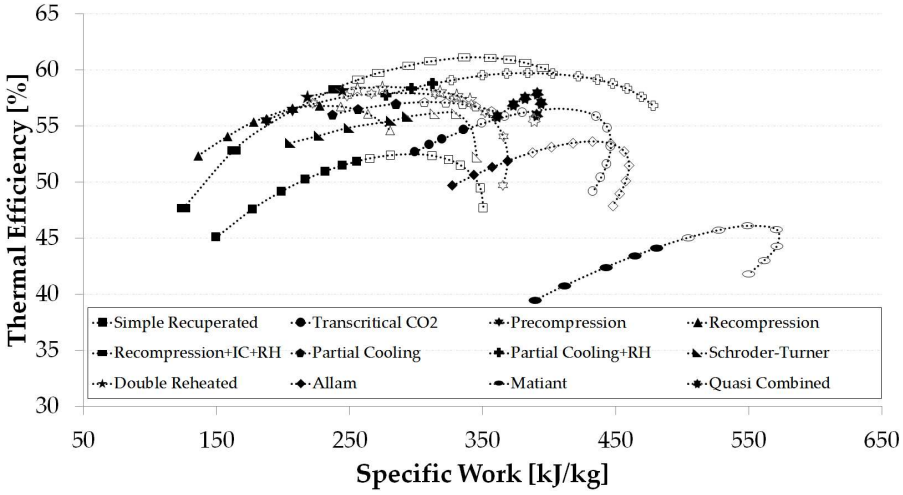

(a) Comparison of cycles operating at TIT=950 ºC.

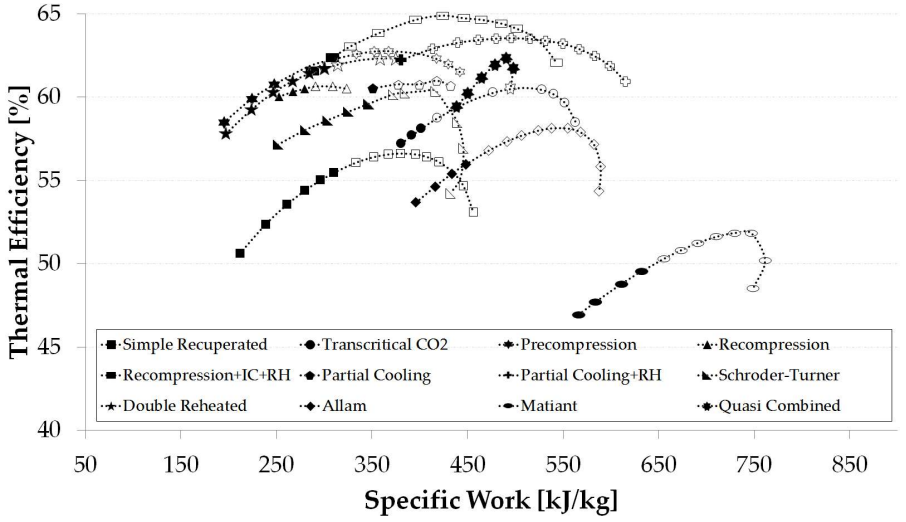

(b) Comparison of cycles operating at TIT=1150 ºC.

Fig. 19. Comparison of cycles operating at TIT=950 ºC and TIT=1150 ºC.

satility of the approach presented in this paper is also highlighted further.

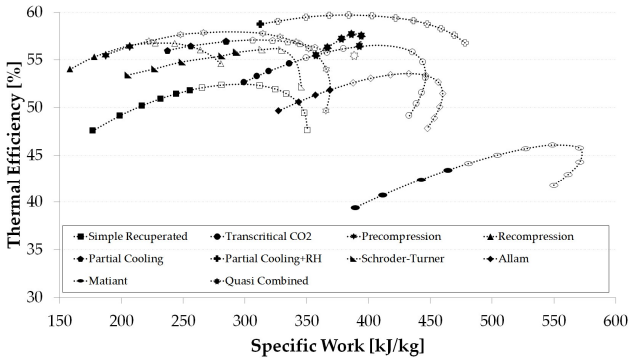

Fig. 20. Comparison of cycles operating at TIT=950 °C. Operating conditions yielding recuperators with hot inlet temperatures higher than 800°C have been removed.

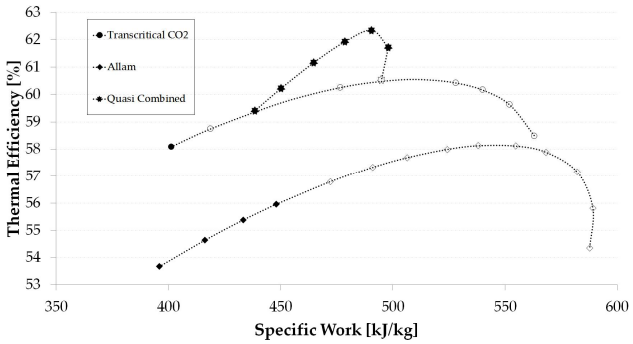

Fig. 21. Comparison of cycles operating at TIT=1150 °C. Operating conditions yielding recuperators with hot inlet temperatures higher than 800°C have been removed.

$$\eta_C = 1 - \frac{T_L}{T_H} \quad , \quad CF = \frac{\eta_{th}}{\eta_C} \tag{1}$$

Based on this figure of merit representing Second Law performance, a new plot of *efficiency* vs. specific work is presented in Fig. 22 for 950ºC. This new chart accounts for the dissimilar cold cycle temperatures, introducing significant changes in the results with respect to the previous analysis. It is immediately observed, in fact, that the *Quasi-Combined* layout, which stood out as one of the most promising cycles in Fig. 20, is no longer interesting. Actually, the apparently very high thermal efficiency was due to an extremely low temperature at compressor inlet and not to a layout with unmatched thermodynamic potential. On the contrary, the *Partial Cooling + RH* configuration exhibits better performance than any other cycle in the comparison, which confirms the results in the First Law approach to the analysis. In this case, the cycle has some inherent advantages over the alternative layouts.

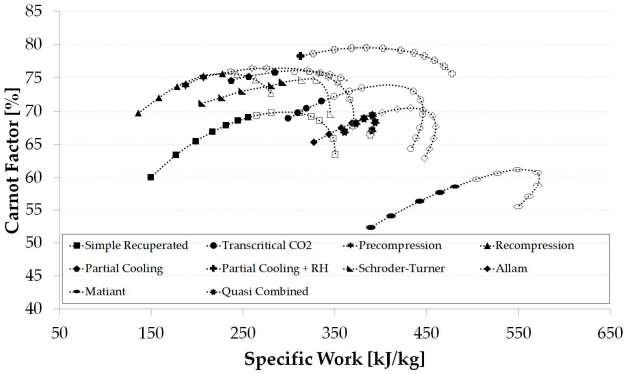

Fig. 22. Comparison of cycles operating at TIT=950 °C considering their Carnot Factor. Operating conditions yielding recuperators with hot inlet temperatures higher than 800°C have been removed.

Carnot Factor Analysis

Table 3 showed that the boundary conditions applied to each cycle were not completely homogeneous. Such difference comes from the need to model disimilar cycles and becomes particularly evident for the compressor/pump inlet conditions in the *Transcritical* CO_2 and the *Quasi-Combined* layouts. Although this is inevitable to model the particular features of these cycles properly (condensation process and cryogenic cooling respectively), it can also be misleading when the comparison relies on the First Law of Thermodynamics only (Figs. 18 to 21).

Such limitation is easily overcome if the Carnot Factor (*CF*) is used. This is the ratio from the thermal efficiency of the cycle (η_{th}) to the thermal efficiency of the Carnot operated between the same extreme temperatures (η_C), Eq. (1).

CONCLUSIONS

This work was originally conceived as a revisit of the systematic thermodynamic analysis of supercritical carbon dioxide cycles carried out by Angelino and co-workers in the early ages of this technology. This approach provided worthwhile information about the possible routes for further efficiency increase and footprint reduction under different boundary conditions: condensing/non-condensing cycles, turbine inlet temperatures and others. Unfortunately, this methodology was, in most cases, abandoned later and substituted by a less thermodynamically sound approach. The consequence of this lack of theoretical foundation has been presented in Fig. 2.

Some interesting conclusions can be drawn from the individual and compared analyses of the twelve sCO_2 cycles

considered. As a general observation, pressure ratio seems to have a weaker influence on thermal efficiency at lower turbine inlet temperatures, as deduced from the lower slope (flatter curves) of the η_{th} vs. W_s lines in Fig. 18(a) in comparison with the same plots in Fig. 19(b). Accordingly, increasing the pressure ratio in the latter set of plots brings about similar enhancements of thermal efficiency and specific work. This was to be expected from the recuperative layout of the cycles and is here confirmed and quantified.

Another important conclusion is that a number of cycles are of no interest at all, regardless of whether or not pressure limits are taken into account. These cycles would be easily identified if an envelope curve were plot by linking the rightmost black markers achieving highest efficiency and specific work. Those cycles falling to the left of this "border" would have no added value and should be disregarded for future analysis (except if there were noteworthy economic reasons that would compensate for a higher heat rate). On the contrary, those intersecting the envelope curve should be kept for further analysis. This is illustrated in Fig. 23 where the grey area stands for the remaining potential to achieve higher efficiency and specific work, should higher operating pressures be enabled in the future.

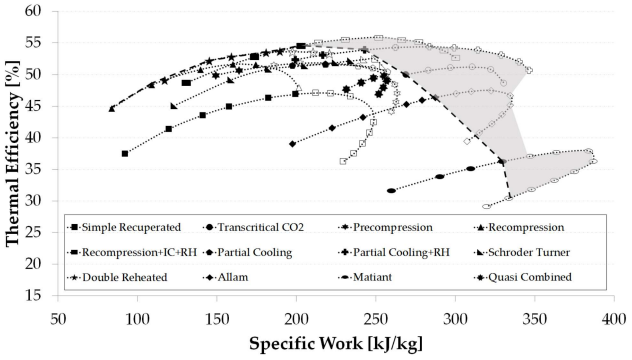

Fig. 23. Comparison of cycles operating at TIT=750 °C, showing envelope curve for 40 MPa and margin for future performance enhancement.

The conclusions above are general but must be taken with care given that the relative positions of the cycles in Figs. 18 and 19 change when turbine inlet pressure changes. Thus, according to the aforedescribed rationale, the *Quasi-Combined* cycle should have been discarded from an analysis at 550ºC. Nevertheless, as turbine inlet temperature increases, the corresponding plot shifts northeast and, by the time this temperature reaches 950ºC, the cycle yields the most leveraged performance (i.e., combination of η_{th} and W_s).

Based on this remark, reporting the most interesting cycle must be accompanied by an indication of the operating and boundary conditions considered, including whether or not technological limits exist. Only with such a complete description, one can state that the *Quasi-Combined* and *Partial Cooling + RH* cycles are the most interesting for applications with turbine inlet temperatures in the range from 900 to 1200ºC, and peak cycle pressure and hot inlet temperature to the recuperator limited to 40 MPa and 800ºC respectively. Moreover, if cryogenic cooling is not available or if the minimum cycle temperature is limited to a minimum value regardless of the cycle layout, then the *Partial Cooling + RH* cycle must be acknowledged as the best choice based on the Carnot Factor analysis. Below 800ºC, the *Recompression + IC + RH* layout yields the best performance and complies with the maximum cycle pressure being lower than 40 MPa.

Finally, when there are no restrictions to pressure and temperature, the analysis shows that the *Recompression + IC + RH* cycle yields highest thermal efficiency irrespective of turbine inlet temperature: 48% at 550ºC, 59% at 750ºC, 61% at 950ºC and 65% at 1150ºC.

References

[1] Feher, E., 1968. "The Supercritical Thermodynamic Power Cycle". *Energy Conversion and Management,* **8**, pp. 85–90.

[2] Angelino, G., 1968. "Carbon Dioxide Condensation Cycles for Power Production". *Journal of Engineering for Power,* **90**(3), pp. 287–295.

[3] Ahn, Y., Bae, S., Kim, M., Cho, S., Baik, S., Lee, J., and Cha, J., 2015. "Review of supercritical CO_2 power cycle technology and current status of research and development". *Nuclear Engineering and Technology,* **47**(6), pp. 647 – 661.

[4] Crespi, F., Gavagnin, G., Sánchez, D., and Martínez, G., 2017. "Supercritical carbon dioxide cycles for power generation: A review". *Applied Energy,* **195**, pp. 152–183.

[5] Angelino, G., 1969. "Real Gas Effects in Carbon Dioxide Cycles.". In ASME 1969 Gas Turbine Conference and Products Show.

[6] Wilson, D., 1998. *The Design of High-Efficiency Turbomachinery and Gas Turbines*. Prentice Hall, New York.

[7] Frutschi, H., 2005. *Closed-Cycle gas turbines. Operating experience and future potential*. ASME Press, New York.

[8] Held, T. J., 2014. Hot day cycle. US Patent 8,783,034.

[9] Nassar, A., Moroz, L., Burlaka, M., Pagur, P., and Govoruschenko, Y., 2014. "Designing Supercritical CO_2 Power Plants Using an Integrated Design System". In ASME 2014 Gas Turbine India Conference, American Society of Mechanical Engineers.

[10] Ahn, Y., Bae, S. J., Kim, M., Cho, S. K., Baik, S., Lee, J. I., and Cha, J. E., 2014. "Cycle layout studies of S-CO2 cycle for the next generation nuclear system application". In Transactions of the Korean Nuclear Society Autumn Meeting.

[11] Yantovski, E., Zvagolsky, K., and Gavrilenko, V., 1995. "The cooperate-demo power cycle". *Energy conversion and management,* **36**(6), pp. 861–864.

[12] Muto, Y., Aritomi, M., Ishizuka, T., and Watanabe, N.,

2014. "Comparison of Supercritical CO2 Gas Turbine Cycle and Brayton CO_2 Gas Turbine Cycle for Solar Thermal Power Plants". In The 4^{th} Supercritical CO_2 Power Cycles Symposium.

[13] Mathieu, P., and Nihart, R., 1999. "Zero-emission MATIANT cycle". *Journal of Engineering for Gas Turbines and Power,* **121**(1), pp. 116–120.

[14] Zhang, N., and Lior, N., 2006. "A novel near-zero CO_2 emission thermal cycle with LNG cryogenic exergy utilization". *Energy,* **31**(10), pp. 1666–1679.

[15] Moisseytsev, A., and Sienicki, J. J., 2009. "Investigation of Alternative Layouts for the Supercritical Carbon Dioxide Brayton Cycle for a Sodium-Cooled Fast Reactor.". *Journal of Engineering for Power,* **239**(7), pp. 1362–1371.

[16] Allam, R., Fetvedt, J., Forrest, B., and Freed, D., 2014. "The Oxy-Fuel, Supercritical CO_2 Allam Cycle: New Cycle Developments to Produce Even Lower-Cost Electricity From Fossil Fuels Without Atmospheric Emissions". In ASME Turbo Expo 2014: Turbine Technical Conference and Exposition, American Society of Mechanical Engineers.

[17] Kulhánek, M., and Dostal, V., 2011. "Thermodynamic analysis and comparison of supercritical carbon dioxide cycles". In The 3^{rd} Supercritical CO_2 Power Cycles Symposium, pp. 24–25.

[18] McClung, A., Brun, K., and Chordia, L., 2014. "Technical and Economic Evaluation of Supercritical Oxy-combustion for Power Generation". In The 4^{th} Supercritical CO_2 Power Cycles Symposium, pp. 1–24.

[19] Serrano Remón, I. P., Linares Hurtado, J. I., Cantizano González, A., and Moratilla Soria, B. Y., 2014. "Enhanced arrangement for recuperators in supercritical CO_2 Brayton power cycle for energy conversion in fusion reactors". *Fusion Engineering and Design,* **89**, pp. 1909–1912.

[20] Dostal, V., and Dostal, J., 2011. "Supercritical CO_2 Regeneration Bypass-Cycle - Comparison to Traditional Layouts". In The 3^{rd} Supercritical CO_2 Power Cycles Symposium, pp. 1–5.

[21] Tuo, H., 2011. "Parametric analysis of a reheat carbon dioxide transcritical power cycle using a low temperature heat source". In 2nd International Conference on Environmental Engineering and Applications, IPCBEE, Vol. 17.

[22] Li, X., Huang, H., and Zhao, W., 2014. "A supercritical or transcritical Rankine cycle with ejector using low-grade heat". *Energy Conversion and Management,* **78**, pp. 551–558.

[23] Johnson, G. A., McDowell, M. W., O'Connor, G. M., Sonwane, C. G., and Subbaraman, G., 2012. "Supercritical CO_2 Cycle Development at Pratt and Whitney Rocketdyne". In ASME Turbo Expo 2012: Turbine Technical Conference and Exposition, American Society of Mechanical Engineers, pp. 1015–1024.

[24] Gatewood, J., Moore, J., Nored, M., Brun, K., and Iyengar, V., 2012. "The Texas Cryogenic Oxy-fuel Cycle (TCO): A Novel Approach to Power Generation with CO_2 Options". In ASME Turbo Expo 2012: Turbine Technical Conference and Exposition, American Society of Mechanical Engineers, pp. 1007–1014.

[25] Purjam, M., Goudarzi, K., and Keshtgar, M., 2016. "A New Supercritical Carbon Dioxide Brayton Cycle with High Efficiency". *Heat Transfer Asian Research.*

[26] Allam, R. J., Palmer, M., Brown, G. W., et al., 2013. System and method for high efficiency power generation using a carbon dioxide circulating working fluid. US Patent 8,596,075.

[27] Padilla, R. V., Too, Y. C. S., Benito, R., McNaughton, R., and Stein, W., 2016. "Thermodynamic feasibility of alternative supercritical CO_2 Brayton cycles integrated with an ejector". *Applied Energy,* **169**, pp. 49–62.

[28] Serrano, I., Linares, J., Cantizano, A., and Moratilla, B., 2013. "A Novel Supercritical CO_2 Power Cycle for Energy Conversion in Fusion Power Plants". *Fusion Science and Technology,* **64**(3), pp. 483–487.

[29] Turchi, C. S., Ma, Z., Neises, T. W., and Wagner, M. J., 2013. "Thermodynamic Study of Advanced Supercritical Carbon Dioxide Power Cycles for Concentrating Solar Power Systems". *Journal of Solar Energy Engineering,* **135**(4), p. 041007.

[30] Mecheri, M., and Le Moullec, Y., 2016. "Supercritical CO_2 Brayton cycles for coal-fired power plants". *Energy,* **103**, pp. 758–771.

[31] Schroder, A. U., 2016. "A Study of Power Cycles Using Supercritical Carbon Dioxide as the Working Fluid". PhD thesis, University of Cincinnati.

[32] Dostal, V., Driscoll, M. J., and Hejzlar, P., 2004. "A supercritical carbon dioxide cycle for next generation nuclear reactors". *Massachusetts Institute of Technology. Dept. of Nuclear Engineering, Cambridge, MA, Paper No. MIT-ANP-TR-100.*

[33] Neises, T. W., and Turchi, C. S., 2014. "Supercritical CO_2 Power Cycles: Design Considerations for Concentrating Solar Power". In The 4^{th} Supercritical CO_2 Power Cycles Symposium, Vol. 2, pp. 9–10.

[34] Coolprop. http://www.coolprop.org. Retrieved November 3^{th} 2016 .

[35] Nellis, G., and Klein, S., 2009. *Heat Transfer.* Cambridge University Press.

[36] Hoopes, K., Snchez, D., and Crespi, F., 2016. "A New Method for Modelling Off-Design Performance of sCO_2 Heat Exchangers Without Specifying Detailed Geometry". In The 5^{th} Supercritical CO_2 Power Cycles Symposium.

[37] Silvestri, G., 2003. Eddystone Station, 325 MW Generating Unit, A Brief History.

[38] Armor, A., 2002. Ultrasupercritical Steam Turbines: Design and Materials Issues for the Next Generation.

[39] McDonald, C., 2003. "The cooperate-demo power cycle". *Applied Thermal Engineering,* **23**(12), pp. 1463–1487.

